Generation of self-induced-transparency gap solitons by modulational instability in uniformly doped fiber Bragg gratings

B. Kalithasan,[1,*] K. Porsezian,[1,†] K. Senthilnathan,[2,‡] and P. Tchofo Dinda[3,§]

[1]*Department of Physics, Pondicherry University, Pondicherry, 605 014 Pondicherry, India*

[2]*Department of Physics, National Institute of Technology, Rourkela, 769 008 Orissa, India*

[3]*Institut Carnot de Bourgogne, UMR 5209 CNRS–Université de Bourgogne, Avenue A. Savary, Boîte Postale 47 870, F-21078 Dijon Cédex, France*

(Received 29 November 2009; published 3 May 2010)

We consider the continuous-wave (cw) propagation through a fiber Bragg grating that is uniformly doped with two-level resonant atoms. Wave propagation is governed by a system of nonlinear coupled-mode Maxwell-Bloch (NLCM-MB) equations. We identify modulational instability (MI) conditions required for the generation of ultrashort pulses in both anomalous and normal dispersion regimes. From a detailed linear stability analysis, we find that the atomic detuning frequency has a strong influence on the MI. That is, the atomic detuning frequency induces nonconventional MI sidebands at the photonic band gap (PBG) edges and near the PBG edges. Especially in the normal dispersion regime, MI occurs without any threshold condition, which is in contrast with that of conventional fiber Bragg gratings. We also perform a numerical analysis to solve the NLCM-MB equations. The numerical results of the prediction of both the optimum modulation wave number and the optimum gain agree well with that of the linear stability analysis. Another main result of the present work is the prediction of the existence of both bright and dark self-induced transparency gap solitons at the PBG edges.

DOI: 10.1103/PhysRevA.81.053802 PACS number(s): 42.65.Wi

I. INTRODUCTION

Modulational instability (MI) is one of the fundamental phenomena in nonlinear physics. It finds plenty of applications in many branches of physics. For instance, in nonlinear fiber optics, this phenomenon is essential, as it helps to generate ultrashot pulses (USPs). In MI, a continuous or a quasicontinuous wave undergoes a modulation of its amplitude or phase in the presence of noise or any other weak perturbation [1–13]. The perturbation can originate from either a quantum noise or a frequency-shifted signal wave. The former and latter are referred to as spontaneous MI and induced MI, respectively. MI occurs under the combined action of group velocity dispersion and self-phase modulation, and this condition is essentially the same for soliton pulse generation. To get more insight, MI may be analyzed in both temporal and frequency domains. In the temporal domain, breakup of the perturbed cw takes place owing to MI (cw undergoes exponential growth), and as a result there is formation of a train of USPs. In the frequency domain, the generation of high-repetition-rate pulse trains resulting from MI can be identified by the growth of a cascade of sidebands. MI in optical fibers was predicted by Hasegawa and Brinkman [3] and experimentally demonstrated by Tai *et al.* [4]. Lots of work on MI has been carried out in the context of optical fiber communications [1]. Very recently, through the MI process, nonconventional sidebands induced by self-induced transparency (SIT) have been reported in a fiber that is uniformly doped by two-level resonant atoms [14]. McCall and Hahn [15] showed that if the energy difference between the two levels of the medium matches the optical wavelength, then coherent absorption and re-emission light occurs. Consequently, the medium becomes optically transparent at this wavelength in the physical process of SIT. SIT solitons are coherent optical pulses propagating through a resonant fiber without loss and distortion. Theoretically, SIT soliton propagation in optical fibers doped with erbium was first shown by Maimistov *et al.* [16–18] and experimentally demonstrated in Refs. [19] and [20].

From a practical point of view, a special type of fiber called fiber Bragg grating (FBG) is better than a conventional telecommunication fiber, as FBG offers a huge amount of dispersion [1,7,8,21]. As in fibers, MI has also been studied in a FBG at low and high power levels for anomalous (upper branches) and normal (lower branches) dispersion regimes, respectively [1,7,8]. MI has been observed experimentally in an apodized grating structure wherein a single pulse has been converted into a train of USPs [9,10]. In addition to temporal instabilities, spatial instabilities have also been studied in a nonlinear bulk medium with Bragg gratings in the presence of Kerr-type nonlinearity [11]. The impact of non-Kerr nonlinearity in terms of MI has also been studied in an FBG where the system possesses cubic-quintic nonlinearities [21]. At this juncture it should be pointed out that in the aforementioned conventional FBGs, MI in the normal dispersion regime has threshold conditions [1,7,8]. To overcome this problem, dynamic grating has been proposed wherein the occurrence of MI was demonstrated experimentally without any threshold condition in the normal dispersion regime [12,13]. Very recently, the role of nonlinearity management in terms of MI has also been investigated, in Refs. [22] and [23].

So far, for PBG structured materials, dynamic grating has been the only choice to achieve MI in a normal dispersion regime with low power without any threshold condition. In general, from the implementation point of view, it may be difficult to achieve USPs in the normal dispersion regime of dynamic FBGs. However, keeping this in mind, we propose

*balathasan2003@yahoo.co.in
†ponz.phy@pondiuni.edu.in
‡senthee12@rediffmail.com
§tchofo@u-bourgogne.fr

to use FBGs doped uniformly with two-level resonant atoms, with which MI can be achieved in a normal dispersion regime at low power and without any threshold condition. In this work, we investigate the occurrence of MI for both anomalous and normal dispersion regimes. Especially, we show that there is no threshold condition for occurrence of MI in the normal dispersion regime. In the detailed analysis, we find that the SIT effect induces nonconventional sidebands in uniformly doped FBGs. In addition, we discuss the formation of SIT solitons near the photonic band gap (PBG) edge. Nonconventional sidebands induced by the SIT effect in the normal dispersion regime and the generation of SIT solitons in terms of the resulting MI are considered to be the main themes of the present paper.

The paper is laid out as follows. In Sec. II, we discuss the necessary theoretical model to describe the propagation of cw in FBGs doped uniformaly with two-level atoms. In Sec. III, we apply linear stability analysis (LSA) to identify MI conditions near the edges of the PBG in both anomalous and normal dispersion regimes. In addition, we perform the dint numerical simulation of nonlinear coupled-mode Maxwell-Bloch (NLCM-MB) equations and then compare MI gain spectra produced by the LSA with MI gain spectra generated by numerical simulation. The next natural step is to discuss the generation of SIT Bragg solitons in terms of the resulting MI maximum gain. We analytically discuss the generation of periodic (cnoidal) waves as well as bright and dark SIT Bragg solitons near the PBG edges in Sec. IV. We conclude in Sec. V.

II. THEORETICAL MODEL

The dynamical behavior of forward (q_+) and backward (q_-) propagation of the modes of an electric field in an FBG uniformly doped with two-level resonant atoms [25–27] is governed by the following coupled-mode equations:

$$i\frac{\partial q_+}{\partial z}+i\frac{\partial q_+}{\partial t}+\delta q_+ +\kappa q_- +\gamma(|q_+|^2+2|q_-|^2)q_+ +\Gamma P_+ =0, \tag{1a}$$

$$-i\frac{\partial q_-}{\partial z}+i\frac{\partial q_-}{\partial t}+\delta q_- +\kappa q_+ +\gamma(2|q_+|^2+|q_-|^2)q_- +\Gamma P_- =0, \tag{1b}$$

where $q_\pm$ and $P_\pm$ are the slowly varying envelopes of the electric field and the resonant polarization, respectively, z is the propagation coordinate, t is the local time, δ is the pulse wave number that detunes from the exact Bragg resonance, κ is the linear coupling coefficient, γ ($=n_2\omega_B/cA_{\text{eff}}$) is self-phase modulation, A_{eff} is the effective core area, $\Gamma=\omega_B/(2nc\epsilon_0)$, n is the linear index of refraction, and ϵ_0 is the vacuum permittivity. The Bloch equations for the resonant polarization P and the population difference W [$=(N_1-N_2)/N_D$], induced by an electromagnetic field Q, are given by [25–27]

$$\frac{\partial P}{\partial t}=i\Delta P-iRWQ, \tag{2a}$$

$$\frac{\partial W}{\partial t}=i\frac{R}{2}(QP^*-Q^*P), \tag{2b}$$

where Δ ($=\omega_r-\omega_B$) is the frequency detuning from the transition frequency of the resonant atoms ω_r to the incoming radiation frequency ω_B ($=2\pi c/\lambda_B$), N_D ($=N_1+N_2$) is the doped density, N_1 and N_2 are the ground-state and upper-state population densities of the two-level atoms, respectively, $R=\mu/\hbar$, where μ is the dipole matrix element of the individual atom and $\hbar$ is Planck's constant divided by 2π, and λ_B is the Bragg wavelength of the grating. In this paper, we consider the homogeneous broadening energy levels of the resonant atoms. The resonant polarization P and the population difference W satisfy the following normalization condition [14,17]:

$$W^2+|P|^2=1, \tag{3}$$

which reflects the conservation of probability in the sense that the total probability of an atom's being found in either the upper or the lower levels is equal to unity. The steady-state solution of Eqs. (2a) and (2b) can be written in the following form:

$$P=\frac{RW}{\Delta}Q, \tag{4a}$$

$$W=\pm\left(1-\frac{|Q|^2}{2p_s}\right), \tag{4b}$$

where $p_s=(\Delta/R)^2$. Here, we have assumed that the field intensity $|Q|^2$ is sufficiently small compared with p_s ($|Q|^2\ll p_s$). The steady-state solution of P and W is obtained so that Eq. (3) is satisfied automatically. Without field-induced polarization, the two-level system population is not inverted, hence the lower sign must be chosen in Eq. (4b) [36]. A general Fourier expansion will lead to an infinite number of coupled equations. In the spirit of the slowly varying envelope approximation, we obtain a closed set of equations by keeping only the leading terms, namely [25]:

$$Q=q_+e^{ik_Bz}+q_-e^{-ik_Bz}, \tag{5a}$$

$$P=P_+e^{ik_Bz}+P_-e^{-ik_Bz}, \tag{5b}$$

$$W=W_0+W_1e^{2ik_Bz}+W_1^*e^{-2ik_Bz}. \tag{5c}$$

Upon substituting Eq. (5) into Eq. (2), we obtain the following coupled equations [24,25]:

$$\frac{\partial P_+}{\partial t}-i\Delta P_+ +iR(q_+W_0+q_-W_1)=0, \tag{6a}$$

$$\frac{\partial P_-}{\partial t}-i\Delta P_- +iR(q_-W_0+q_+W_1^*)=0, \tag{6b}$$

$$\frac{\partial W_0}{\partial t}-i\frac{R}{2}(q_+P_+^*+q_-P_-^*-q_+^*P_+-q_-^*P_-)=0, \tag{6c}$$

$$\frac{\partial W_1}{\partial t}-i\frac{R}{2}(q_+P_-^*-q_-^*P_+)=0. \tag{6d}$$

The steady-state solutions of Eqs. (6a)–(6d) can be found through Eq. (4). Equations (1) and (6) are the governing equations, from which we obtain the necessary conditions for the occurrence of MI in both normal and anomalous dispersion regimes.

III. LINEAR STABILITY ANALYSIS

In this section, we use LSA to investigate the occurrence of MI. Thus, the prime aim of LSA is to perturb the cw solution. Then we analyze whether this small perturbation grows or decays with propagation. It is obvious that LSA is valid as long as the perturbation amplitude remains low compared with the cw beam amplitude. The steady-state solutions of Eqs. (1) and

(6) can be written as follows:

$$q_{\pm} = U_{\pm} e^{i\phi z}, \tag{7a}$$

$$P_{\pm} = \Upsilon_{\pm} U_{\pm} e^{i\phi z}, \tag{7b}$$

$$W_j = s_j, \tag{7c}$$

where $j = 0,1$, $U_+ = \sqrt{p_0/(1+f^2)}$, $U_- = \sqrt{p_0/(1+f^2)}\, f$, $\Upsilon_{\pm} = (R/\Delta)s_{\pm}$, $s_0 = -[1-(p_0/2p_s)]$, $s_1 = fU_+^2/(2p_s)$, $s_+ = -\{1-[(1+2f^2)s_1/f]\}$, $s_- = -\{1-[(2+f^2)s_1/f]\}$, and p_0 is the total power. Here, $f = q_-/q_+$ can be positive or negative. For values of $|f| < 1$, the backward wave dominates. On substituting Eqs. (7) into Eqs. (1a) and (1b), we obtain the following nonlinear dispersion relation:

$$\phi = -\frac{\kappa}{2f}(1-f^2) - \frac{1}{2}(1-f^2)H + \frac{1}{2}(\Upsilon_+ - \Upsilon_-)\Gamma, \tag{8a}$$

$$\delta = -\frac{\kappa}{2f}(1+f^2) - \frac{3}{2}\gamma p_0 - \frac{1}{2}(\Upsilon_+ + \Upsilon_-)\Gamma, \tag{8b}$$

where $H \equiv \gamma p_0/(1+f^2)$ is an effective nonlinear parameter. Here, we ensure that the preceding nonlinear dispersion relation leads to the conventional FBG case if we switch off the SIT effect ($\Gamma = 0$) [1]. In addition, the resulting nonlinear dispersion relation reduces to the linear dispersion relation when the nonlinear effect is turned off ($p_0 = 0$). Now, through this linear dispersion relation, we explore the role of dopants, that is, SIT effect by means of dispersion curve. Figures 1(a) and 1(b) describe the linear ($p_0 = 0$) dispersion curves for FBG uniformly doped with two-level resonant atoms and conventional FBG. In Figs. 1(a) and 1(b), dotted, dashed, and dot-dashed lines illustrate the dispersion curves of uniformly doped FBG for $\Delta = \pm 10^{12}$ Hz, $\Delta = \pm 10^{13}$ Hz, and $\Delta = \pm 10^{14}$ Hz, respectively, and the solid lines represent the dispersion curves of the conventional FBG [for $\Gamma = 0$ in Eq. (8)]. For comparatively lower values of the atomic detuning parameter Δ, the dispersion curves do undergo shift-up [Fig. 1(a)] or shift-down [Fig. 1(b)], depending on the negative or positive sign of Δ. For instance, for $\Delta = \pm 10^{14}$ Hz, the linear dispersion curves [dot-dashed lines in Figs. 1(a) and 1(b)] nearly close to the conventional FBG. From Figs. 1(a) and 1(b), it is very clear that the characteristics of the linear dispersion curves have been dramatically changed by the atomic detuning frequency Δ. The detuning parameter δ of the cw beam from the Bragg frequency determines the values of f, which in turn fixes the values of ϕ in Eqs. (8a) and (8b). The group velocity (V_G) inside the grating also depends on f and is given by $V_G = d\delta/dq = (1-f^2)/(1+f^2)$. The upper ($f < 0$) and lower ($f > 0$) branches

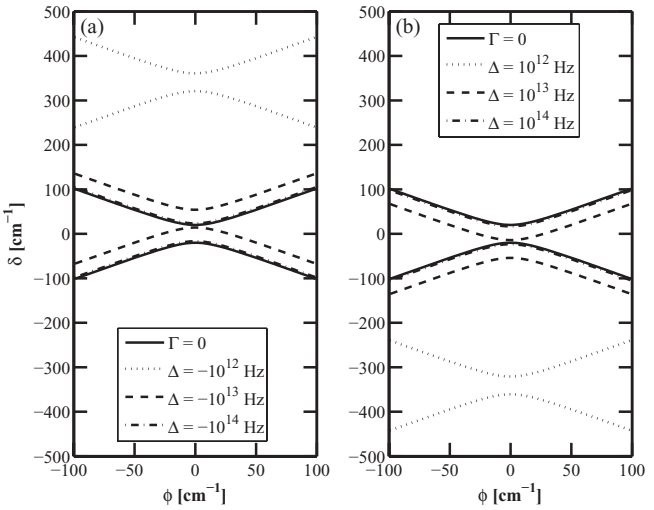

FIG. 1. Linear dispersion relation curve for $\kappa = 20$ cm^{-1}, $\Gamma = 0$ (solid line), $\Delta = \pm 10^{12}$ Hz (dotted line), $\Delta = \pm 10^{13}$ Hz (dashed line), $\Delta = \pm 10^{14}$ Hz (dot-dashed line), and $p_0 = 0$. The solid curve represents the linear dispersion relation for conventional FBG ($\Gamma = 0$).

of the dispersion curve represent the anomalous and normal dispersion regimes, respectively. Two edges of the PBG occur at $f = \pm 1$.

A. Modulational instability gain spectra

The LSA of steady-state solutions can be examined by introducing perturbed fields of the following form:

$$q_{\pm} = [U_{\pm} + a_{\pm}\cos(Kz + \Omega t) + ib_{\pm}\sin(Kz + \Omega t)]e^{i\phi z}, \tag{9a}$$

$$P_{\pm} = \Upsilon_{\pm}[U_{\pm} + c_{\pm}\cos(Kz + \Omega t) + id_{\pm}\sin(Kz + \Omega t)]e^{i\phi z}, \tag{9b}$$

$$W_0 = s_0[1 + w_0\cos(Kz + \Omega t)], \tag{9c}$$

$$W_1 = s_1[1 + w_+\cos(Kz + \Omega t) + iw_-\sin(Kz + \Omega t)], \tag{9d}$$

where $a_{\pm}$, $b_{\pm}$, $c_{\pm}$, $d_{\pm}$, w_0, and $w_{\pm}$ are real amplitudes of infinitesimal perturbations, K is the perturbed wave number, and Ω is the respective eigenvalue. Substituting expressions (9a)–(9d) into Eqs. (1)–(6) and performing the linearization, we obtain the 11 nontrivial equations for the perturbed fields $a_{\pm}$, $b_{\pm}$, $c_{\pm}$, $d_{\pm}$, w_0, and $w_{\pm}$, which can be written in an 11×11 matrix form. This set has a nontrivial solution only when the 11×11 determinants formed by the coefficient matrix vanish as follows:

$$\begin{vmatrix}
m_{11} & 0 & 0 & 0 & 0 & 0 & m_{17} & -\kappa & m_{19} & 0 & 0 \\
0 & m_{22} & 0 & 0 & 0 & 0 & \kappa & m_{28} & 0 & m_{210} & 0 \\
0 & 0 & m_{33} & 0 & 0 & 0 & s_0 & -s_1 & s_+ & 0 & m_{311} \\
0 & 0 & 0 & m_{44} & 0 & 0 & -s_1 & s_0 & 0 & s_- & 0 \\
0 & 0 & 0 & 0 & m_{55} & 0 & m_{57} & m_{58} & m_{59} & m_{510} & 0 \\
0 & 0 & 0 & 0 & 0 & m_{66} & m_{67} & m_{68} & m_{69} & m_{610} & 0 \\
m_{71} & m_{72} & m_{73} & 0 & 0 & 0 & m_{77} & 0 & 0 & 0 & 0 \\
m_{81} & m_{82} & 0 & m_{84} & 0 & 0 & 0 & m_{88} & 0 & 0 & 0 \\
-s_0 & s_1 & -s_+ & 0 & 0 & m_{96} & 0 & 0 & m_{99} & 0 & 0 \\
s_1 & -s_0 & 0 & -s_- & 0 & 0 & 0 & 0 & 0 & m_{1010} & 0 \\
m_{111} & m_{112} & m_{113} & m_{114} & 0 & 0 & 0 & 0 & 0 & 0 & m_{1111}
\end{vmatrix} = 0, \tag{10}$$

where

$$m_{11} = -m_{77} \equiv K - \Omega, \quad m_{17} \equiv f\kappa + \frac{\Gamma R s_+}{\Delta},$$
$$m_{19} = -m_{73} \equiv -\frac{\Gamma R s_+}{\Delta},$$
$$m_{22} = m_{88} \equiv K + \Omega, \quad m_{28} \equiv -\frac{\kappa}{f} - \frac{\Gamma R s_-}{\Delta},$$
$$m_{210} = m_{84} \equiv \frac{\Gamma R s_-}{\Delta},$$
$$m_{33} = -m_{99} \equiv \frac{\Omega s_+}{\Delta}, \quad m_{311} = -m_{96} \equiv -s_1 U_-,$$
$$m_{44} = m_{1010} \equiv \frac{\Omega s_-}{\Delta},$$
$$m_{55} \equiv \Omega s_0, \quad m_{57} = -m_{59} \equiv -\frac{R^2 U_+ s_1}{\Delta},$$
$$m_{58} = m_{510} \equiv -\frac{R^2 U_- s_+}{\Delta},$$
$$m_{66} = m_{1111} \equiv \Omega s_1,$$
$$m_{67} = -\frac{m_{610}}{f} = -m_{111} = -\frac{m_{114}}{f} \equiv -\frac{R^2 U_- s_-}{2\Delta},$$
$$m_{68} = -f m_{69} = m_{112} = f m_{113} \equiv \frac{R^2 U_+ s_+}{2\Delta},$$
$$m_{71} \equiv 2H - f\kappa - \frac{\Gamma R s_+}{\Delta},$$
$$m_{72} = m_{81} \equiv \kappa + 4fH, \quad m_{82} \equiv 2Hf^2 - \frac{\kappa}{f} - \frac{\Gamma R s_-}{\Delta}.$$

It is well established that MI occurs when there is an exponential growth rate (gain) in the amplitude of the perturbed wave, which in turn implies the existence of a nonvanishing imaginary part in the complex parameter Ω. For the case of FBG uniformly doped with two-level resonant atoms, MI occurs when there is exponential growth in the amplitude of the perturbed wave, which implies the existence of a nonvanishing largest imaginary part in the complex parameter $G(K) \equiv \Omega$. For $\Upsilon_\pm = 0$, the eigenvalue in Eq. (10) is tantamount to that found in [1] and [7].

Here, we aim to display the MI gain spectra, as functions of K, Δ, f, and H, for both the anomalous (upper branch for $f < 0$) and the normal (lower branch for $f > 0$) dispersion regimes. We examine here various kinds of behaviors that arise when the sign and the magnitude of the atomic resonant detuning parameter Δ are varied. For demonstration purposes, we consider the following physical parameters: $\gamma = 0.002\,\mathrm{W^{-1}\,m^{-1}}$, $\kappa = 20\ \mathrm{cm^{-1}}$, $\lambda_B = 1.55 \times 10^{-6}\,\mathrm{m}$, $\epsilon_0 = 8.854 \times 10^{-12}\,\mathrm{F\,m^{-1}}$, $\mu = 1.4 \times 10^{-32}\,\mathrm{Cm}$, $\hbar = 1.0545 \times 10^{-34}$ J s, and $N_D = 8 \times 10^{24}\,\mathrm{m^{-3}}$. Here, we carry out the MI analysis for different values of the atomic resonant detuning parameter, $\Delta = \pm 10^{12}$, $\pm 10^{13}$, and $\pm 10^{14}$ Hz, as we are interested in investigating the influence of the atomic resonant detuning parameter. Figures 2(a)–2(d) represent the MI gain spectra for both the PBG edge and near the PBG edge for various values Δ in the range $\pm 10^{12}$ to $\pm 10^{14}$ Hz. Figures 2(a) and 2(c) illustrate the MI gain spectra at the PBG edge and near the PBG edge, respectively, for a negative sign of the atomic resonant detuning parameter Δ, with various values (-10^{12} to -10^{14} Hz), whereas Figs. 2(b) and 2(d) show the MI gain spectra for a positive sign of Δ (10^{12} to 10^{14} Hz). The solid lines in

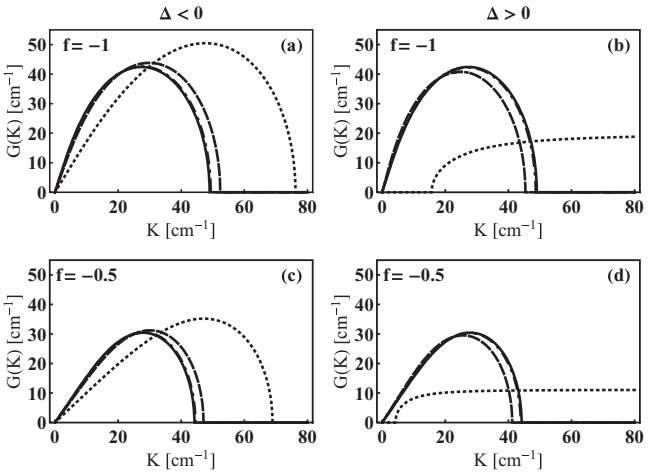

FIG. 2. MI gain spectrum obtained from the LSA for the anomalous dispersion regime (upper branch) for $\kappa = 20\ \mathrm{cm^{-1}}$, $H = 0.5\kappa$, $\Upsilon_\pm = 0$ (solid line), $\Delta = \pm 10^{12}$ Hz (dotted line), $\Delta = \pm 10^{13}$ Hz (dashed line), and $\Delta = \pm 10^{14}$ Hz (dot-dashed line). The solid line represents the MI gain spectrum of conventional FBG ($\Upsilon_\pm = 0$).

Fig. 2 represent the MI gain spectra for the conventional FBG ($\Gamma = 0$). When $\Delta = \pm 10^{14}$ Hz (dot-dashed lines), the MI gain spectra coincide with conventional FBG. From this physical process, we infer that the system ceases to hold the effect of SIT for relatively higher values of the atomic resonant detuning parameter, $\Delta = \pm 10^{14}$ Hz. Thus, the impact can be realized only for relatively lower values of the atomic resonant detuning parameter ($|\Delta| < 10^{14}$). In Figs. 2(a) and 2(c), dotted lines illustrate that the corresponding optimum wave number (the wave number at which maximum gain occurs) and the peak gain (maximum gain) are relatively large for $\Delta = -10^{12}$ Hz. However, increasing the magnitude of the negative values of Δ leads to a shrinkage of the MI gain spectra, whereas both the peak gain and the bandwidth decrease rapidly for $\Delta < 0$. From Figs. 2(b) and 2(d), it is obvious that both the MI gain and the bandwidth of the MI gain spectra increase with the atomic resonant detuning parameter, Δ ($>10^{12}$ Hz). For $\Delta = 10^{12}$ Hz (dotted lines), all the wave numbers with a magnitude below a certain values are stable, while all wave numbers with a larger magnitude are unstable, which is in great contrast with the conventional FBG [1,7,8]. Another important point is that the MI bandwidth becomes infinite for $\Delta = 10^{12}$ Hz. Here, we infer that the bandwidth is infinite for $\Delta \leqslant 10^{12}$ Hz, whereas the bandwidth is finite when $\Delta > 10^{12}$ Hz. An infinite bandwidth is not the signature of an ordinary MI process. In other words, such a gain spectrum with infinite bandwidth corresponds, in practice, to a system with a reduced ability to generate the MI process. The dashed lines depict the MI gain spectra for $\Delta = \pm 10^{13}$ Hz. In addition to the two-dimensional (2D) plots in Fig. 2, the 3D plots in Figs. 3(a) and 3(b) represent the MI sidebands for a low power ($H < \kappa$). The peak gain and the bandwidth of the MI sidebands increase as the effective nonlinear parameter H increases. Figures 2 and 3 clearly show that the peak gain is relatively higher at the top of the PBG ($f = -1$) than near the PBG edge ($f < 0$).

Now we turn to the MI process in the normal dispersion (lower branch) regime. The purpose of this paper is to

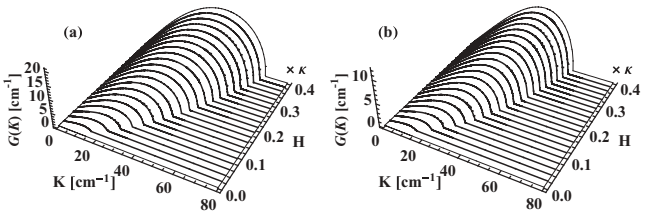

FIG. 3. MI gain spectrum obtained from the LSA for the anomalous dispersion regime [(a) $f = -1$ and (b) $f = -0.5$] for $\kappa = 20\ \mathrm{cm}^{-1}$ and $\Delta = -10^{12}$ Hz.

overcome the finite threshold conditions for the conventional FBG MI process in the normal dispersion regime. The conventional FGB MI process has threshold conditions in the normal dispersion regime as follows [7,8]. (i) The instability required a finite threshold condition, $H > \kappa/2$, where H is the effective nonlinear parameter. Thus, if the input power is sufficiently low, then the continuous wave signal is stable against small perturbations: only when the power exceeds threshold condition ($H > \kappa/2$) is the signal unstable. (ii) For $f > 0.447$, all the wave numbers with a magnitude below a certain value are stable, while all wave numbers with a larger magnitude are unstable. In this case, wave numbers are infinite. Most of the unstable wave numbers are finite at $f > 0.447$. Figures 4 and 5 represent the occurrence of MI in the normal dispersion regime. Also, the resulting MI gain spectra strongly depend on the atomic detuning parameter Δ in the normal dispersion regime (Fig. 4). Figures 4(a)–4(d) illustrate the following important features: One can easily see that the MI gain spectra are close to the conventional FBG for larger magnitude values of the atomic resonant detuning parameter, $|\Delta| > 10^{12}$ Hz. From this physical process, we conclude that the uniformly doped FBG system ceases to hold the effect of SIT for $\Delta = \pm 10^{13}$ Hz (dashed lines) and $\Delta = \pm 10^{14}$ Hz (dot-dashed lines). In this case, we find that all wave numbers with a magnitude below a certain value are stable, while all wave numbers of a larger magnitude

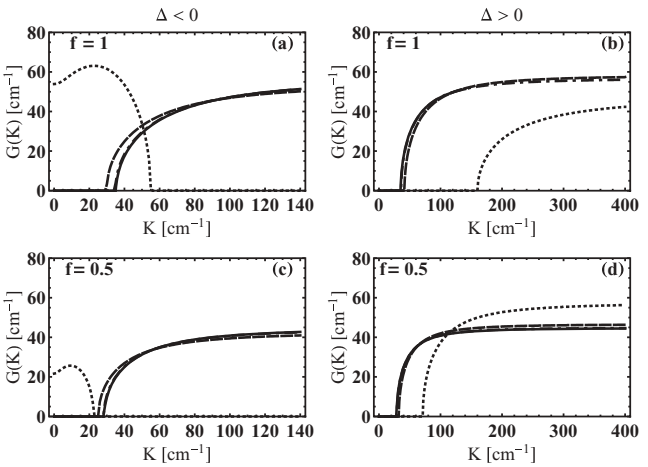

FIG. 4. MI gain spectrum obtained from the LSA for the normal dispersion regime (lower branch) for $\kappa = 20\ \mathrm{cm}^{-1}$, $H = 1.5\kappa$, $\Upsilon_{\pm} = 0$ (solid line), $\Delta = \pm 10^{12}$ Hz (dotted line), $\Delta = \pm 10^{13}$ Hz (dashed line), and $\Delta = \pm 10^{14}$ Hz (dot-dashed line). The solid line represents the MI gain spectrum of conventional FBG ($\Upsilon_{\pm} = 0$).

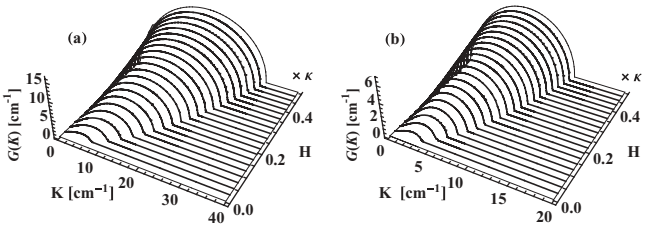

FIG. 5. MI gain spectrum obtained from the LSA for the normal dispersion regime [(a) $f = 1$ and (b) $f = 0.5$]. The physical parameters are $\kappa = 20\ \mathrm{cm}^{-1}$ and $\Delta = -10^{12}$ Hz.

are unstable. This behavior confirms the similarity to the conventional FBG where the MI process has a finite threshold condition [1,7,8]. The role of the SIT effect can be realized only close to resonance for $\Delta = \pm 10^{12}$ Hz (dotted lines). In the normal dispersion regime, the SIT effect can be nullified by large magnitude values of the atomic resonant detuning parameter ($|\Delta| > 10^{12}$ Hz), which means that uniformly doped FBG acts as a conventional FBG. In the normal dispersion regime, the atomic resonant detuning parameter Δ can induce nonconventional MI sidebands where there is no threshold condition [dotted lines in Figs. 4(a) and 4(c)]. Here, we observe that all wave numbers are unstable with finite wave number and the instability exists even at an offset wave number ($K = 0$). In general, the nonconventional MI processes have a substantial advantage over the ordinary conventional MI process, that is, they offer more possibilities to obtain a large MI bandwidth.

Figures 5(a) and 5(b) show that the MI gain spectra can occur without any threshold conditions such as low power ($H < \kappa$) and all wave numbers are unstable in the normal dispersion regime. The peak value of the gain spectrum grows and the sidebands broaden as the effective nonlinear parameter H increases, which is represented in Fig. 5. From this physical process, the MI gain spectra depend strongly on the input power. Figures 5(a) and 5(b) represent the MI gain spectra at the bottom (normal dispersion regime) of the PBG edge ($f = 1$) and near the PBG edge ($f = 0.5$), respectively.

Near the resonance, $\Delta = -10^{12}$ Hz [dotted lines in Figs. 4(a), 4(c), and 5], we find nonconventional MI processes in the lower branch (normal dispersion regime) of uniformly doped FBG, which are induced by the atomic detuning parameter Δ. In this case, the MI process differs qualitatively from conventional FBG in two respects. The first of these is that this MI process has no threshold, which in turn implies that the continuous wave is unstable. The second major difference is the shape of the MI gain spectrum. In the lower branch, all wave numbers with all values are unstable, and instability can occur at a finite wave number. Thus, such kind of abnormal behavior should be contrasted with the conventional FBG where the MI process has a threshold.

B. Comparison with modulational instability spectra obtained from direct simulations

In the previous section, MI was analyzed by means of LSA. Here, we aim to compare the predictions with direct simulation of the NLCM-MB equations, adding small initial perturbations to cw states, for the cases of both the anomalous and the normal dispersion regimes. It is shown by the typical examples

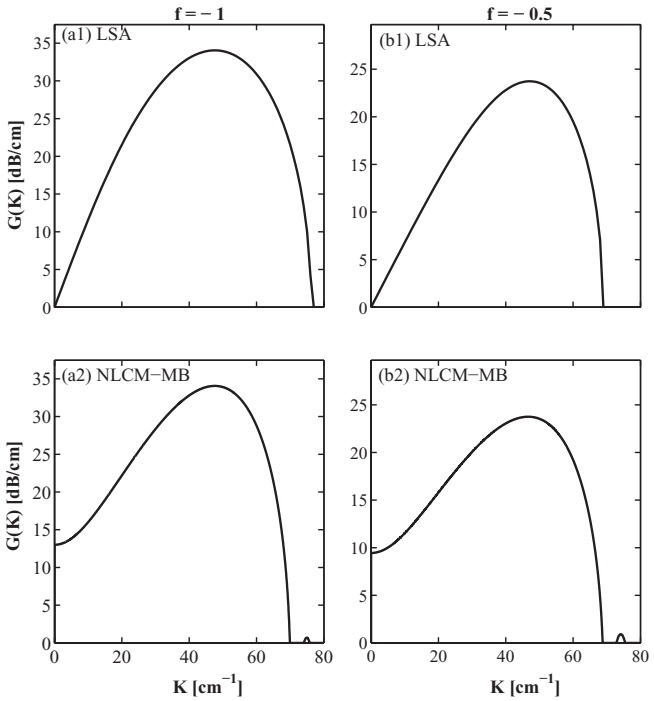

FIG. 6. MI gain spectra (a1, b1) obtained from the LSA for the anomalous dispersion regime and (a2, b2) restored from direct simulations of the NLCM-MB equations. The physical parameters are $\kappa = 20\ \mathrm{cm}^{-1}$, $H = 0.5\kappa$, and $\Delta = -10^{12}$ Hz.

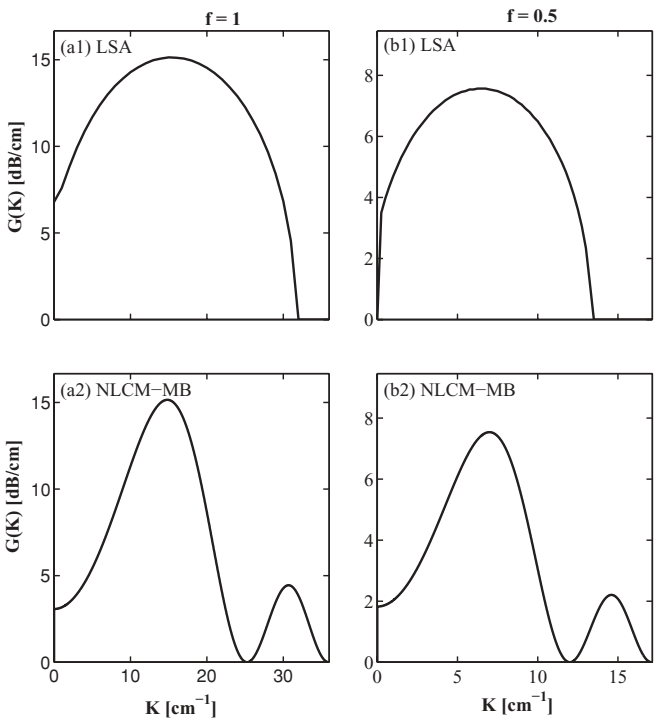

FIG. 7. MI gain spectra (a1, b1) obtained from the LSA for the normal dispersion regime and (a2, b2) restored from direct simulations of the NLCM-MB equations. The physical parameters are $\kappa = 20\ \mathrm{cm}^{-1}$, $H = 0.5\kappa$, and $\Delta = -10^{12}$ Hz.

displayed in Figs. 6 and 7 that the gain spectra, especially the optimum wave number and the peak gain, as predicted by the LSA, agree with their counterparts that can be extracted from direct numerical results (Table I). The stability of the steady-state solution given by Eq. (7) was tested by adding small initial perturbations to it. Simulations of NLCM-MB equations with such initial conditions were performed (using Matlab) by means of the split-step Fourier method. The MI gain was extracted from results of simulations which show the growth of the intensity fluctuations seeded by the small initial perturbations.

IV. GENERATION OF SELF-INDUCED TRANSPARENCY SOLITONS NEAR PHOTONIC BAND GAP EDGES ($f = \pm 1$)

Having discussed the MI conditions, we proceed to find the optimum gain with a minimum power, which will be utilized to discuss the generation of SIT solitons near the PBG of uniformly doped FBG. Gap and Bragg solitons have been extensively investigated by many research groups in FBG [28–31] and investigations of these exciting entities are still alive. In uniformly doped FBGs, the grating-induced dispersion balances with both the material Kerr nonlinearity and the resonant effects determined by the Bloch equations. The resulting solitons are known as SIT Bragg solitons, which are essentially distortionless optical pulses. Because of the balance based on the pure grating dispersion, the doping concentration and the atomic detuning frequency can dramatically change the characteristics of a SIT Bragg soliton when the carrier frequency is close to the original edges of the band gap. Distortionless SIT Bragg soliton pulses have been investigated in a uniformly doped nonlinear PBG structure [25–27]. The authors found both the gap SIT solitons in a periodic array of thin layers of resonant two-level atoms separated by half-wavelength nonabsorbing dielectric layers, that is, a resonantly absorbing Bragg reflector [32–36].

Mantsyzov and Kuzmin [37] studied nonlinear pulse propagation in a discrete 1D medium made of two-level atoms. Kozhekin and Kurizkai [33] extended the model just discussed to a continuous medium in which thin layers of resonant atoms were placed at regular intervals inside the periodic dielectric medium. Aközbek and John [25] investigated the properties of SIT solitary waves in a 1D nonlinear periodic structure doped uniformly with resonant two-level atoms. In addition, they reported SIT gap solitons whose central frequency was detuned near the PBG edge. It has been mentioned that these SIT solitons could be useful in optical communications and optical computing since the dopant density and atomic detuning frequency dramatically change the characteristics of

TABLE I. Optimum wave number (K_{opt}) and peak gain (G_{peak}) obtained from Figs. 6 and 7.

		K_{opt} (cm^{-1})		G_{peak} (dB/cm)	
S. no.	f	LSA	NLCM-MB	LSA	NLCM-MB
1	−1.0	48.00	48.00	34.05	34.05
2	−0.5	47.00	47.00	23.74	23.74
3	0.5	15.00	15.00	15.14	15.14
4	1.0	06.75	06.75	07.57	07.57

SIT gap solitons. Recently, Tseng and Chi [26] investigated the existence of a moving SIT pulse train in a uniformly doped PBG structure. These authors reduced the NLCM-MB equations into equivalent NLCM equations called effective NLCM equations. They solved the effective NLCM equations and investigated the aforementioned pulse-train soliton solutions in a uniformly doped nonlinear periodic structure. Following similar work, they also discussed the coexistence of a SIT soliton and a Bragg soliton in a nonlinear PBG medium doped uniformly with inhomogeneously broadening two-level atoms. For this purpose, they derived the effective nonlinear Schrödinger equation (NLS) equation from the effective NLCM equations to discuss the SIT Bragg soliton near the PBG structure.

In this section, we discuss how to generate SIT solitons near a PBG edge. If the grating parameters are nearly constant over the spectral bandwidth of the pulse and the central frequency of the incident pulse is close to but outside the grating stop band, NLCM-MB equations can be reduced to nonlinear Schrödinger-Maxwell-Bloch (NLS-MB) equations having the following form [25,26]:

$$i\frac{\partial q}{\partial t} - \frac{\beta_2^g}{2}\frac{\partial^2 q}{\partial z^2} + \gamma_g |q|^2 q + \Gamma P = 0, \tag{11a}$$

$$\frac{\partial P}{\partial t} - i\Delta P + iRqW = 0, \tag{11b}$$

$$\frac{\partial W}{\partial t} - i\frac{3R}{4}(qP^* - q^*P) = 0, \tag{11c}$$

where $\beta_2^g = 1/\kappa$ and $\gamma_g = 3\gamma$. To start with, we consider the general solution of the form $q(z,t) = A(\chi)e^{i(kz-\omega t)}$, $P(z,t) = [u(\chi) + iv(\chi)]e^{i(kz-\omega t)}$, and $W(z,t) = \eta(\chi)$, where $\chi \equiv t - (z/V)$, V is the soliton velocity, k the wave number, and ω the frequency of the solution sought. Upon substituting this ansatz into Eqs. (11a)–(11c) and separating the real and imaginary parts, we obtain

$$-\left(\frac{\beta_2^g}{2V^2}\right)\frac{d^2A}{d\chi^2} + \gamma_g A^3 + \left(\frac{\beta_2^g k^2}{2} + \omega\right)A + \Gamma u = 0, \tag{12a}$$

$$\left(1 + \frac{k\beta_2^g}{V}\right)\frac{dA}{d\chi} + \Gamma v = 0, \tag{12b}$$

$$\frac{du}{d\chi} + (\Delta + \omega)v = 0, \tag{12c}$$

$$\frac{dv}{d\chi} - (\Delta + \omega)u + RA\eta = 0, \tag{12d}$$

$$\frac{d\eta}{d\chi} - \left(\frac{3}{2}\right)RAv = 0. \tag{12e}$$

Further, substituting v from Eq. (12b) into Eq. (12e), we can eliminate the population variable,

$$\eta = -1 - \left(\frac{3R\left(1 + k\beta_2^g/V\right)}{4\Gamma}\right)A^2 \tag{13}$$

and inserting u, v, and η from Eqs. (12a), (12b), and (13) into Eqs. (12c) and (12d), we arrive at a second-order equation:

$$\frac{d^2A}{d\chi^2} = \alpha_{11}A + \alpha_{12}A^3, \tag{14a}$$

$$\frac{d^2A}{d\chi^2} = \alpha_{21}A - \alpha_{22}A^3, \tag{14b}$$

where

$$\alpha_{11} \equiv \frac{2V^2(\Delta + 2\omega) + Vk[Vk + 2(\Delta + \omega)]\beta_2^g}{\beta_2^g},$$

$$\alpha_{12} \equiv \frac{2\gamma_g V^2}{\beta_2^g},$$

$$\alpha_{21} \equiv \frac{V^2\left[(\Delta + \omega)\left(\beta_2^g k^2 + 2\omega\right) - 2R\Gamma\right]}{2V^2 + (2kV + \Delta + \omega)\beta_2^g},$$

$$\alpha_{22} \equiv \frac{V\left[3R^2\left(V + k\beta_2^g\right) - 4V(\Delta + \omega)\gamma_g\right]}{2[2V^2 + (2kV + \Delta + \omega)]\beta_2^g}.$$

We can derive the solitary-wave solutions from Eqs. (14a) and (14b). It is clear that Eqs. (14a) and (14b) can be equivalent only under the following conditions: $\alpha_{11} = \alpha_{21}$ and $\alpha_{21} = -\alpha_{22}$. The integration of Eq. (14b) produces an equation for the traveling wave,

$$\left(\frac{dA}{d\chi}\right)^2 = \alpha_{21}A^2 - \frac{1}{2}\alpha_{22}A^4 + 2C, \tag{15}$$

where C is an arbitrary integration constant. Equation (15) can be solved in terms of the Jacobi elliptic functions. In particular, the choice of $C = m^2(1-m^2)\alpha_{21}^2/(2m^2-1)^2\alpha_{22}$ yields a solution for cnoidal waves (written in terms of elliptic functions cn, sn, and dn, which depend on modulus m):

$$q(z,t) = \sqrt{p_0}\,\mathrm{cn}\left[\frac{t-(z/V)}{T_0}, m\right]e^{i(kz-\omega t)},$$

$$\begin{aligned} P(z,t) = \frac{\sqrt{p_0}}{\Gamma}\Bigg(&\varrho_1\,\mathrm{cn}\left[\frac{t-(z/V)}{T_0}, m\right] \\ &- \varrho_2\mathrm{cn}^3\left[\frac{t-(z/V)}{T_0}, m\right] \\ &- i\left(\frac{V + k\beta_2^g}{VT_0}\right)\mathrm{sn}\left[\frac{t-(z/V)}{T_0}, m\right] \\ &\times \mathrm{dn}\left[\frac{t-(z/V)}{T_0}, m\right]\Bigg)e^{i(kz-\omega t)}, \end{aligned} \tag{16}$$

$$W(z,t) = -1 - \left(\frac{3Rp_0(V + k\beta_2)}{2V\Gamma}\right)\mathrm{cn}^2\left[\frac{t-(z/V)}{T_0}, m\right],$$

where we have defined

$$T_0 \equiv \sqrt{\frac{2m^2-1}{\alpha_{21}}},$$

$$\varrho_1 \equiv \frac{(m^2+m-1)\beta_2^g}{2V^2T_0^2} - \frac{\beta_2^g}{2}k^2 + \omega,$$

$$\varrho_2 \equiv \gamma_g p_0 + \frac{m(m+1)\beta_2^g}{2T_0^2V^2},$$

and the elliptic modulus is implicitly determined by power p_0 through the following relation:

$$p_0 \equiv \frac{2m^2\alpha_{21}}{(2m^2-1)\alpha_{22}}.$$

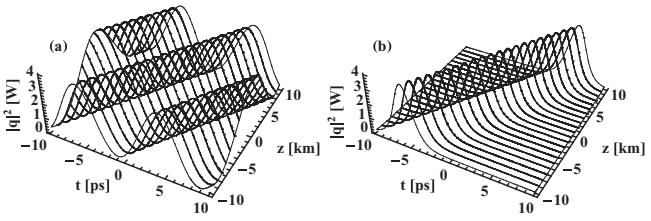

FIG. 8. (a) Intensity profile of the cn ($m = 0.4$) solution and (b) intensity profile of the bright ($m = 1$) SIT soliton solution, for $f = -1$, $p_0 = 2$ W, $k = 12$ m^{-1}, $\omega = 0.7$ Hz, and $V = 0.4$ m s^{-1}.

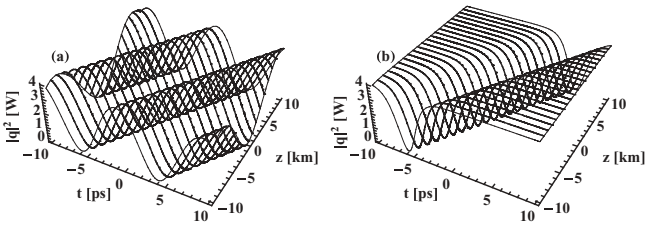

FIG. 9. (a) Intensity profile of the sn ($m = 0.4$) solution and (b) intensity profile of the dark ($m = 1$) SIT soliton solution, for $f = -1$, $p_0 = 2$ W, $k = 12$ m^{-1}, $\omega = 0.7$ Hz, and $V = 0.4$ m s^{-1}.

Parameter T_0, which determines the period of the cnoidal-wave solution, can be expressed in terms of p_0 as

$$T_0 = \sqrt{\frac{2m^2}{p_0\alpha_{22}}}. \tag{17}$$

Figure 8(a) displays a typical example of the local power distribution corresponding to the cn solution in the anomalous (top PBG edge) dispersion regime. Further, Fig. 8(b) shows the profile of the bright SIT gap soliton, which is obtained from solution (16) in the limit of $m = 1$. Actually, these soliton solutions were reported in Refs. [14] and [25]. Similarly, if the integration constant is chosen to be $C = -(m\alpha_{21})^2/(m^2+1)^2\alpha_{22}$, Eq. (15) generates another exact periodic solution in terms of function sn:

$$\begin{aligned} q(z,t) &= \sqrt{p_0}\,\mathrm{sn}\left[\frac{t-(z/V)}{T_0},m\right]e^{i(kz-\omega t)},\\ P(z,t) &= -\frac{\sqrt{p_0}}{\Gamma}\left(\sigma_1\,\mathrm{sn}\left[\frac{t-(z/V)}{T_0},m\right]\right.\\ &\quad+\sigma_2\mathrm{sn}^3\left[\frac{t-(z/V)}{T_0},m\right]\\ &\quad+i\left(\frac{V+k\beta_2^g}{VT_0}\right)\mathrm{cn}\left[\frac{t-(z/V)}{T_0},m\right]\\ &\quad\left.\times\,\mathrm{dn}\left[\frac{t-(z/V)}{T_0},m\right]\right)e^{i(kz-\omega t)},\\ W(z,t) &= -1-\left(\frac{3Rp_0\left(V+k\beta_2^g\right)}{2V\Gamma}\right)\mathrm{sn}^2\left[\frac{t-(z/V)}{T_0},m\right], \end{aligned} \tag{18}$$

where the following relations should be imposed on the parameters:

$$\begin{aligned} p_0 &\equiv \frac{2m^2\alpha_{21}}{(m^2+1)\alpha_{22}}, \quad T_0 \equiv \sqrt{\frac{m^2+1}{\alpha_{21}}},\\ \sigma_1 &\equiv \frac{(m+1)\beta_2^g}{2V^2T_0^2}+\frac{\beta_2^g}{2}k^2+2\omega,\\ \sigma_2 &\equiv \gamma_g p_0-\frac{m(m+1)\beta_2^g}{2V^2T_0^2}. \end{aligned}$$

The intensity distribution in the sn solution, in the anomalous dispersion regime, is displayed in Fig. 9(a). In addition, in Fig. 9(b) we show the profile of the limit solution with $m = 1$, which corresponds to a dark SIT gap soliton in the anomalous dispersion regime. Similarly, we can generate the cnoidal solutions, as well as their limit forms, for $m = 1$, which corresponds to the bright and dark SIT gap solitons in the case of the normal (bottom PBG edge) dispersion ($\beta_2^g > 0$) regime. Our results describe that both bright and dark SIT gap solitons can be generated in the cases of the anomalous and normal dispersion regimes [14]. This should be contrasted with the well-known situations in Ref. [38], where bright and dark SIT gap solitons exist, solely with the anomalous and normal dispersion regimes. On the contrary, it is known that bright and dark solitons coexist in the model based on a periodic array of narrow layers of resonant two-level atoms, which simultaneously plays the role of the Bragg reflector [34,35]. It is noteworthy that a Painlevé analysis could not reveal the existence of dark solitons in the NLS-MB system [39], while the present results make it possible to find them in both cases, normal and anomalous dispersion.

From an experimental viewpoint, we have calculated important and interesting physical parameters such as pulse power (p_0) and pulse width (T_0). Based on the arguments, we believe that SIT gap solitons could be generated experimentally in FBG uniformly doped with resonant two-level atoms. Experimental observation of SIT gap solitons in uniformly doped FBG is an attractive subject, which could lead to practical expansions of gap solitons in the vast area of light-wave systems. In contrast to the fiber SIT soliton, SIT gap solitons can be realized experimentally since uniformly doped FBGs have a length of only a few centimeters, owing to the large dispersion; this is long enough for generating SIT gap solitons.

V. CONCLUSION

By means of MI analysis, we have identified the MI conditions required to generate USPs in uniformly doped two-level FBG systems. It should be pointed out that there is a threshold condition for the occurrence of MI in the normal dispersion regime of a conventional FBG, whereas in the case of dynamic grating the same thing can be achieved without any threshold condition. However, this is difficult to realize practically. Keeping this in mind, we proposed and identified MI conditions, in the normal dispersion regime, which do not require any power threshold condition. Thus it is quite possible to achieve MI in the normal dispersion regime of a uniformly doped FBG, which is in contrast to conventional FBG. We have

also performed a numerical analysis to solve the governing NLCM-MB equations. The numerical results of the prediction of the optimum modulation wave number and optimum gain agree well with those of the LSA. In addition, the generation of periodic and exact (bright and dark) SIT gap solitary waves has been investigated at the PBG edges ($f = \pm 1$). We have also derived a relation between the total input power and the pulse width, which demonstrates the possibility of generating SIT gap solitary waves.

ACKNOWLEDGMENTS

The authors are grateful to S. V. M. Sathyanarayana for fruitful discussions. This work was carried under Contract No. IFC/3504-F/2005/2064 between the IFCPAR and the Universities of Burgundy and Pondicherry. K.P. also wishes to thank the CSIR, DST-DFG, and Ramanna Fellowship (DST), Government of India, for financial support through major projects.

[1] G. P. Agrawal, *Applications of Nonlinear Fiber Optics* (Academic Press, New York, 2001).
[2] A. Hasegawa, Opt. Lett. **9**, 288 (1984).
[3] A. Hasegawa and W. F. Brinkman, IEEE J. Quantum Electron. **16**, 694 (1980).
[4] K. Tai, A. Hasegawa, and A. Tomita, Phys. Rev. Lett. **56**, 135 (1986).
[5] L. A. Ostrovskii, Sov. Phys. JETP **24**, 797 (1967).
[6] G. Millot, E. Seve, S. Wabnitz, and J. M. Haelterman, J. Opt. Soc. Am. B **15**, 1266 (1998).
[7] C. M. de Sterke, J. Opt. Soc. Am. B **15**, 2660 (1998).
[8] F. Kh. Abdullaev, S. A. Darmanyan, and J. Garnier, in *Progress in Optics XLIV*, edited by E. Wolf (Elsevier, Amsterdam, 2002).
[9] B. J. Eggleton, C. M. de Sterke, and R. E. Slusher, J. Opt. Soc. Am. B **14**, 2980 (1997).
[10] B. J. Eggleton, C. M. de Sterke, A. B. Aceves, J. E. Sipe, T. A. Strasser, and R. E. Slusher, Opt. Commun. **149**, 267 (1998).
[11] N. M. Lichinitser, C. J. McKinstrie, C. M. de Sterke, and G. P. Agrawal, J. Opt. Soc. Am. B **18**, 45 (2001).
[12] S. Pitios, M. Haelterman, and G. Millot, Opt. Lett. **26**, 780 (2001).
[13] S. Pitios, M. Haelterman, and G. Millot, J. Opt. Soc. Am. B **19**, 782 (2002).
[14] B. Kalithasan, K. Porsezian, P. Tchofo Dinda, and B. A. Malomed, J. Opt. A Pure Appl. Opt. **11**, 045205 (2008).
[15] S. L. McCall and E. L. Hann, Phys. Rev. Lett. **18**, 908 (1967).
[16] A. I. Maimistov and E. A. Manykin, Sov. Phys. JETP **58**, 685 (1983).
[17] A. I. Maimistov, A. M. Basharov, S. O. Elyutin, and Yu. M. Sklyarov, Phys. Rep. **191**, 1 (1990).
[18] A. I. Maimistov, B. A. Malomed, and A. Desyatinkov, Phys. Lett. A **254**, 179 (1999).
[19] M. Nakazawa, Y. Kimura, K. Kurokawa, and K. Suzuki, Phys. Rev. A **45**, R23 (1992).
[20] M. Nakazawa, K. Suzuki, Y. Kimura, and H. Kubota, Phys. Rev. A **45**, R2682 (1992).
[21] K. Porsezian, K. Senthilnathan, and S. Devipriya, IEEE J. Quantum Electron. **41**, 789 (2005).
[22] J. Ancemma, K. Senthilnathan, K. Porsezian, and P. Tchofo Dinda, J. Opt. A Pure Appl. Opt. **11**, 015203 (2009).
[23] F. Kh. Abdullaev, A. A. Abdumalikov, and R. M. Galimzyanov, Physica D **238**, 1345 (2009).
[24] I. Bar-Joseph and Y. Silberberg, Phys. Rev. A **36**, 1731 (1987).
[25] N. Aközbek and S. John, Phys. Rev. E **58**, 3876 (1998).
[26] H. Y. Tseng and S. Chi, Phys. Rev. E **66**, 056606 (2002).
[27] H. Y. Tseng and S. Chi, IEEE J. Sel. Top. Quantum Electron. **8**, 681 (2002).
[28] A. B. Aceves and S. Wabnitz, Phys. Lett. A **141**, 37 (1989).
[29] A. B. Aceves, Chaos **10**, 584 (2000).
[30] D. N. Christodoulides and R. I. Joseph, Phys. Rev. Lett. **62**, 1746 (1989).
[31] C. M. de Sterke and J. E. Sipe, in *Progress in Optics XXXIII*, edited by E. Wolf (Elsevier, Amsterdam, 1994).
[32] B. I. Mantsyzov, Phys. Rev. A **51**, 4939 (1995).
[33] A. Kozhekin and G. Kurizki, Phys. Rev. Lett. **74**, 5020 (1995).
[34] A. E. Kozhekin, G. Kurizki, and B. A. Malomed, Phys. Rev. Lett. **81**, 3647 (1998).
[35] T. Opatrny, B. A. Malomed, and G. Kurizki, Phys. Rev. E **60**, 6137 (1999).
[36] G. Kurizki, A. E. Kozhekin, and B. A. Malomed, in *Progress in Optics XLII*, edited by E. Wolf (Elsevier, Amsterdam, 2001).
[37] B. I. Mantsyzov and R. N. Kuz'min, Sov. Phys. JETP **64**, 37 (1986).
[38] K. Porsezian and K. Senthilnathan, Chaos **15**, 037109 (2005).
[39] K. Nakkeeran, J. Phys. A Math. Gen. **33**, 7007 (2000).